

An experimental study of acoustic emissions from active surface degradation in planetary gears

Enrique Caso¹, Alfonso Fernandez-del-Rincon, Pablo Garcia, Alberto Diez-Ibarbia, Javier Sanchez-Espiga

Department of Structural and Mechanical Engineering, ETSIT University of Cantabria, Spain

Abstract

In this article, the detection of high frequency elastic waves, known as acoustic emission (AE), is used to correlate the events derived from the gear mesh with the surface wear and the operational behaviour in a planetary gearbox. In this regard, AE monitoring is a method that is able to provide information about the friction in the contact between surfaces in relative motion, which enables to employ a monitoring technology that overcomes the lack of sensitivity of traditional technologies under certain working conditions. Therefore, the investigation of the AE generated during the degradation of active gear surfaces can clarify how this process affects the performance in gearboxes. From the results, it has been stated that modifications in the active surfaces are barely reflected through traditional condition indicators (CI), such as AE frequency spectrum and AE signal envelope frequency spectrum, and same processing with accelerometry signals. It has been also observed that AE event width, or event lifetime, related with the gear meshing its a suitable indicator to monitor gear active surfaces. In this respect, a CI related to the AE event width and based in data reduction algorithm is proposed for gears monitoring with AE. For this work, characteristics of the complex studied system, as sensor position or cyclic periods inherent to the planetary gearbox, are assessed and highlighted as important factors in order to develop a valid monitoring.

Keywords: Acoustic Emission, Planetary Gearboxes, Condition Monitoring, Degradation

¹casoe@unican.com

Nomenclature

<i>AE</i>	Acoustic Emission	<i>FFT</i>	Fast Fourier Transform
<i>CI</i>	Condition Indicator	<i>GMF</i>	Gear Mesh Frequency
<i>ESSP</i>	Equally Spaced Sequentially Phased	<i>PG</i>	Planetary Gearbox
<i>EWI</i>	Event Width Indicator	<i>RMS</i>	Root Mean Square

1. Introduction

The application of acoustic emission (AE) in the monitoring of rotating machinery has shown promising results during its brief lifetime. It emerges as a research field in the middle of the 20th century focused in the microstructure material analysis of cracks and dislocations. It was not until the 1980s that AE was employed as nondestructive testing inspection tool in the industry, especially in the aerospace and petrochemical sectors [1]. In its beginnings, the AE was mainly focused in the monitoring of pressurized structures, as vessels and pipes, for leakage identification and location. Recently, after this initial usage, the AE has been transferred to the machinery monitoring, from static structures to systems with dynamic components as geared transmissions.

Gears are susceptible to degradation in the teeth flanks by phenomena as wear or pitting. In this regard, optical microscopy inspections and profile measurements of gear surfaces has been used by the scientific community in order to track the active surfaces behaviour [2]. However, the main disadvantage of these methods is that the gearbox must be stopped and opened at regular intervals in order to perform the tests. Another option is the oil debris inspection, which is a method that allows to supervise the gears degradation and can be implemented by on-line monitoring of changes in the lubricant parameters [3, 4]. Furthermore, vibration analysis has been used to study the pitting progression in spur gears [5]. On the other hand, AE monitoring has been investigated and compared with traditional accelerometry by [6, 7]. The former concluded that the AE RMS results have shown better sensitivity

than vibration RMS for pitting detection in worm gearboxes. However, the latter observed that the presence of pitting in worm gears can be identified by the variation of the vibration pattern. Later, in [8], AE sensors and acceleration sensors have been compared for early pitting degradation showing an advantage for the acoustic technology due to its higher bandwidth.

The main thesis of AE generation related with the gear mesh involves the interaction of asperities of the engaged teeth surfaces [9]. The asperities, present in the surfaces because of the inherent roughness, provoke rupture and deformation when they contact with opposite surface asperities. Consequently, this process generates acoustic waves and the variations in the asperity distribution over the surface introduce randomness. Additionally, modifications in the gear contact behaviour, such as misalignments, have resulted in alterations in the AE signals [10]. Therefore, AE seems to be a good technology for monitoring surface damage due to its sensitivity to the contact interaction [11]. Nevertheless, lack of experimental proof have led to take into account the importance of other possible source mechanisms in the AE generation during the gear mesh, such as lubricant pressure perturbation, changes in the sliding/rolling condition, backlash, tooth deformation and tooth impact [12].

Few works have assessed the AE signal sensitivity to surface seeded defects or wear progression involving roughness variations in gearboxes. The elimination of material under deformation because of the defect presence in the tooth active surface could omit previous shown events in the AE signal [13]. Alternatively, surface behaviour and the AE RMS have been correlated with the removed material in a similar experiment [14]. Defects can remain distinguishable despite the elimination of surface material after the defect is generated. The tooth surface degradation has been evidenced with AE monitoring by using condition indicator analysis. These degradation processes are shown in the signal RMS tendencies [15]. Different stages related with the active surface behaviour have been identified by using AE in spur gears with pitting, showing much better sensitivity of the damage progression than accelerometry. In comparison to hard surfaces, softer surfaces after the initial wearing stage generate lower AE signal RMS levels, followed by an increasing tendency when the damage starts to appear [16]. The propagation of pitting has also been viewed by event counting over a threshold [17]. The damage of the gear surface has been studied in planetary gearboxes as validation of denoising algorithms [18]. The inappropriate sensor emplacement in the experiments has probably led to refuse the AE advantages in surface degra-

dation monitoring [19]. A recent work, correlating AE signals and surface degradation, has shown the good sensitivity to changes. By considering the phases of gear mesh sequence, a more precise information of AE during teeth interaction has been obtained, employing a parallel shaft transmission with spur gears [20]. To these days, the application of AE technique to monitor planetary gearboxes (PG) is scarce and mainly used to detect artificial defects, such as partially or totally removed tooth [21] and cuts in bearing elements [22], which are not representative of the real defects present in PG operating conditions.

Within this framework, in this manuscript, an experimental study is carried out to monitor the surface damage process using AE in a PG, emulating wind turbine operating conditions. The degradation of the active surfaces is achieved by the natural degradation of a planetary gear without surface treatment. Thus, the varying conditions in terms of active surface behaviour and AE signals are correlated. Moreover, relevant information for the analysis is provided by the gear surfaces inspection using optical photography and the oil debris examination. Therefore, the article contribute to diffuse experimental results obtained under different conditions and to propose explanatory hypothesis. The inaccurate description of the degradation growth obtained by traditional signal analyses leads to propose a new approach for the monitoring. The novelty of this paper is based on the study of the AE event width, or event lifetime, proposed as an important parameter capable of representing the gear active surface contact mechanisms according to the experimental results. For this reason, a new CI to represent the event width in PG is established, providing good results for the degradation process description.

After this introduction, the test bench is presented and preliminary tests with AE signals are assessed to achieve a rigorous monitoring in Sec. 2. The experimental set-up and test methodology are defined in Section 3. The results are displayed in Section 4, starting by an overview of sun gear degradation process and its influence in the generated signals. This description is correlated with signal analysis. Traditional methods are employed, such as condition indicators (CIs), frequency spectrum and signal envelope frequency spectrum, complemented with a comparison to vibration signals, and a new CI is defined in terms of AE event width. Finally, conclusions are made in Section 5. Additional considerations regarding PG morphology and AE technology are provided in Appendix A.

2. Test bench and preliminary tests

The aim of the present paper is to study with AE sensors the progression of active surfaces damage in a PG. Previous works experience has highlighted the importance of some particularities that must be carefully studied in advance to assure the appropriate setting to obtain valuable results and its repeatability. Therefore, AE signals and PG characteristics are preliminarily considered in this section before the main experimental set up is exposed.

2.1. Test bench

The PG employed for the experiments is a back-to-back transmission with two identical planetary stages in a power recirculation configuration (see Fig. 1) [25]. The power recirculation is allowed by the connection of both stages planet-carrier and sun gears with coaxial shafts. Just one of this stages is employed for the degradation tests, maintaining the other one in adequate conditions as auxiliary system to introduce the load. The load is introduced into the PG by an applied torque. The torque can be varied by adding or subtracting masses to a load arm that is connected to the free ring of the auxiliary stage.

In the PG test stage, the sun gear is the input of the system and the planet carrier is the output. An internally toothed ring gear (fixed annulus or ring) allows the planet carrier, a disk-shaped holding element, to rotate around the sun gear. Three planets are mounted in their respective carrier pins through bearings. The movement in the planets is a sum of its rotation and the relative rotation of the planet center, fixed to the carrier, around the sun. Planet gear rotates on the carrier in opposite direction of the sun. On the other hand, the planet center moves in the same direction than the sun, rotating with the planet carrier.

Table 1: Gear numbers of teeth in the employed PG.

Gear	Sun Z_S	Planet Z_P	Ring Z_R
Number of teeth	16	24	65

Planets are equally-spaced mounted in the planet-carrier with identical planet angular spacing ($\psi_i = \psi = 2\pi/3$). According to Eq. A.1, this transmission exhibits a sequential mesh phasing, being classified as an Equally

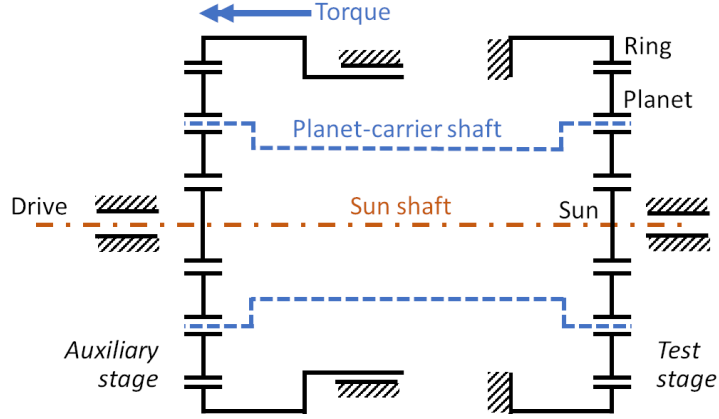


Figure 1: Scheme of the employed PG test bench.

Spaced Sequentially Phased (ESSP) PG. Therefore, there is one third phase delay between each planet engagement.

Given the gears number of teeth, the number of revolutions for a complete PG cycle can be obtained with the angular speeds relation (Eq. A.5).

$$\begin{aligned}\dot{\theta}_S &= \dot{\theta}_C \left(\frac{65}{16} + 1 \right) = \dot{\theta}_C \frac{81}{16} \\ \dot{\theta}_P &= \dot{\theta}_C \left(1 - \frac{65}{24} \right) = \dot{\theta}_C \frac{-41}{24}\end{aligned}\tag{1}$$

where the values of Table 1 are substituted in Eq. A.5.

The PG would need 91 sun revolutions or 48 planet carrier revolutions to complete the “complete PG cycle”, as a result of Eq. 1. For low-speed operation, the time to perform a complete acquisition of this interval would be in order of minutes. For example, 20.22 seconds are needed for the repetition of the exact gears position at a sun shaft speed of 270 rpm, being the GMF equal to $57.78Hz$ (Eq. A.6).

2.2. AE sensor position and resulting signals

The position of the AE sensor must be examined for the monitoring because of AE wave attenuation and acoustic sources overlap. Gearbox AE signal levels are affected by the lubrication film thickness and/or the modification of the couplant layer properties between sensor and the machine [26].

Acquired AE signals are greatly affected by sensor positioning. The acoustic waves travel from the source to the sensor suffering attenuation, reflection, and wavefront interference. Depending on the measurement position, certain process could be neglected. This is due to the acoustic waves transfer path. The sensor sensitivity to one emission source is influenced by component interfaces in its path and by the presence of other acoustic sources, closer to the sensor or with higher intensity. The pressure variations in the sensor plate are generated by the waves reaching this point over the surface, hence one specific source could be hidden under the summation of AE sources present during the PG operation.

Two positions, as can be seen in Figure 2, have been selected in the test bench for the AE sensors, denoted by:

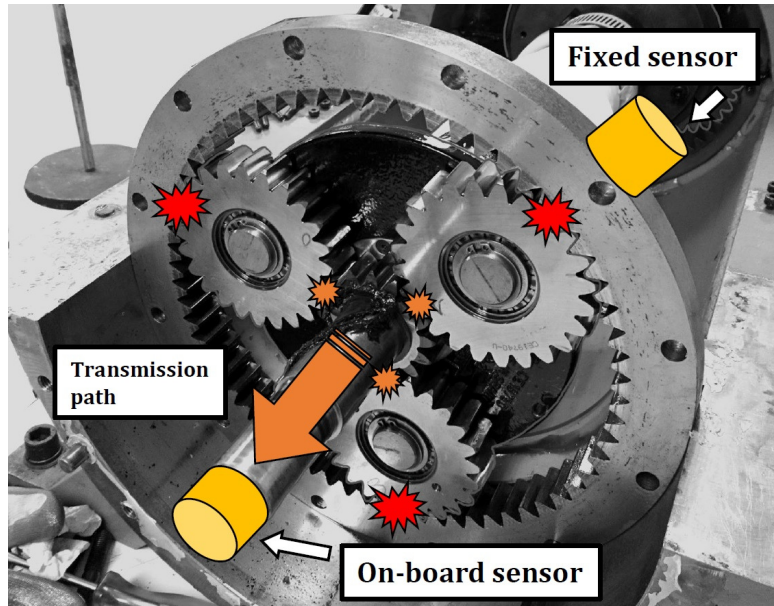


Figure 2: Sensor positions in the partially dismantled PG.

Fixed sensor The sensor is set fixed to the external surface of the ring gear, where the meshing between planets and ring is the most noticeable acoustic source due to the absence of interfaces. The distance between contacts and sensor varies due to the relative movement and therefore the waves attenuation.

On-board sensor This sensor set in the shaft enables a direct transmission path from sun-planets interaction. A device is developed to hold the sensor in contact with the shaft edge, incorporating a slip ring, to connect the sensor and the acquisition board.

AE signals from both positions, fixed and on-board sensor, are preliminarily compared during the normal PG test bench operation with gears in good health conditions. This preparatory analysis allows to identify the main sources of the acoustic waves reaching each position and their suitability to be employed for the signal analysis.

In the fixed sensor signals, amplitude modulation is shown (see Fig. 3). The higher amplitudes coincide with proximity between sensor and source. Consequently, the valleys appear in the signal when the planets are away from the sensor. The amplitude peaks can reach over ten times the amplitude in the valleys. This ratio remains approximately constant along the signal. While the planet is close to the sensor, the main contribution comes from planet-ring mesh. Nevertheless, other sources magnitude could be enough to be observed in the low amplitude valleys. Therefore, the fixed sensor would be able to detect information from low intensity sources during these periods.

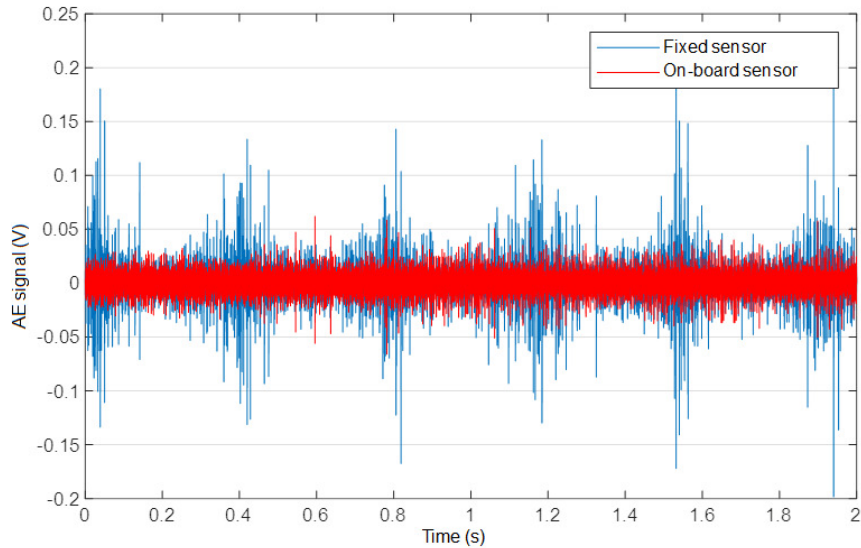


Figure 3: Signals from both fixed and on-board AE sensor position.

In the on-board sensor, a continuous amplitude level signal is shown (Fig. 3). This signal exhibits the same amplitude as the observed during the

modulation valleys in the fixed sensor signals. The invariability of the relative distance between sensor and planet centres produce no amplitude modulation in the signal.

AE envelope spectrum allows a frequency analysis providing similar representation of the machine behaviour than vibration analysis. This analysis has shown a good fault detection capacity using AE signals [27]. Related sun frequencies are shown in the on-board sensor envelope, not in the fixed one. The carrier frequency dominates the fixed sensor spectrum. The GMF frequency is observable in both sensor data, correlating envelope information with gear mesh.

The two spectrograms in Fig. 4 express an example of the different main contribution in each channel. A period of time corresponding to two times the inverse of the GMF is plotted. Therefore, the sun-planets load sharing is repeated twice. The frequency spectrum scope in these plots is limited to 150-175 kHz, where high intensity periodic events have been identified. This band corresponds to the characteristic frequency in the sensor where perturbations are highlighted. The planet sequential mesh phasing provokes three peak events, in place of the expected single event if the planets would have contacted simultaneously.

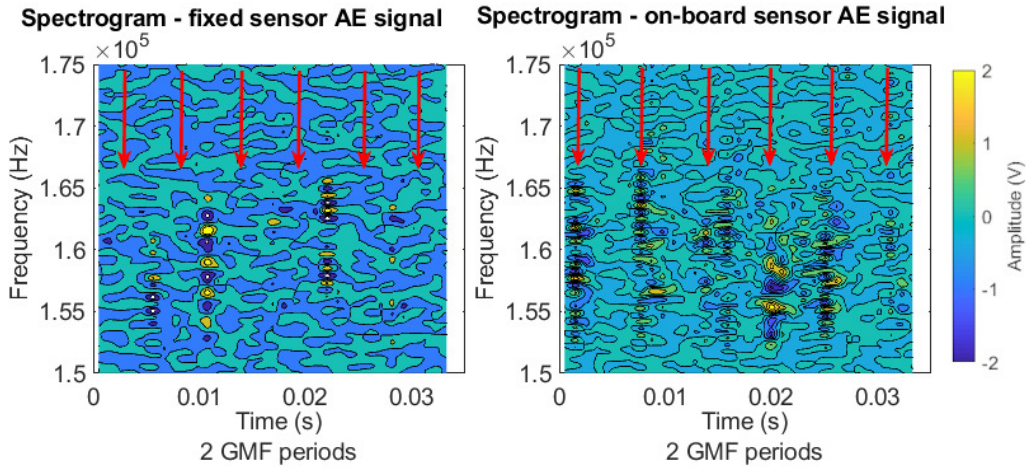


Figure 4: Spectrogram showing the AE time-frequency excitation using fixed (left) and on-board sensor (right).

Six high intensity bands should appear equidistantly in both spectrograms. This behaviour is reproduced in the on-board sensor spectrogram.

Wave intensity reach the sensor with similar magnitude for every gear mesh period. However, one of the bands is highlighted in the fixed sensor, corresponding with the nearest planet. These results display the main activity of sun-planet interaction in the on-board sensor for the above-mentioned reasons.

2.3. Gear selected for degradation test

Next decision that has to be taken before performing the degradation analysis is which element of the transmission favours more the degradation. All the facts lead to the sun gear, as the element that has more contacts per cycle. Nonetheless, as a preliminary test, the degradation of one planet was performed in order to validate this hypothesis, to check the equipment sensitivity and allow us to introduce concepts about AE signal and ESSPPG characteristics useful for the subsequent result analysis. In this regard, a non-treated planet was introduced, keeping the rest of original PG components unchanged. The test consists on the AE signal acquisition at a brief normal PG operation under stationary load and speed conditions. A light degradation is induced in the replaced planet (it is named “planet #1”). Gear active surfaces are easily eroded obtaining different contact behaviours. Thus, it is possible to establish correlations with the AE signal observed patterns. The simultaneous degradation of all components would affect the results interpretation because of the merge of signal perturbations.

The non-treated planet, planet #1, is clearly identified through AE signals (Fig. 5). Amplitude modulation appears because of the pass of this planet near the fixed sensor at the carrier frequency. The planet #1 identification is achieved despite the wave attenuation in its path to the fixed sensor. Higher AE signals are generated by this gear due to its different contact characteristics, rising above the maximum levels obtained with original gears. The sequential mesh phasing allows to study the expected AE signals separately for each planet.

Short distance of the transfer paths avoid significant delays in the wave arrival time, which could merge sequential events. The attenuation with the distance of each planet interaction could be observed separately regarding each planet meshing phase in the AE signal. In order to obtain more accurate results a tachometer is employed. The tachometer allows to transform the time domain signals into angular domain, expressing them in terms of the angle rotated by the carrier respect the ground.

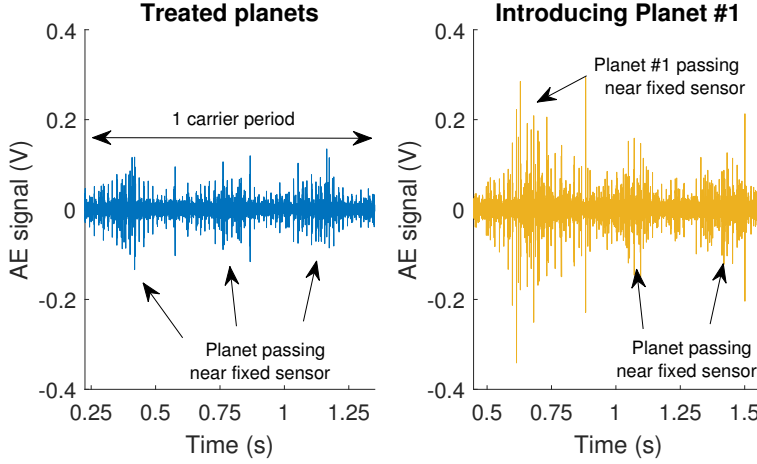


Figure 5: Time domain AE signals with 3 treated planets (left) and Planet #1 plus 2 treated planets (right) for the fixed sensor at 270 rpm and 600 Nm.

As a ESSP PG transmission has been employed (see Appendix A.1), each planet meshing corresponds to a different point along the line of action, existing one third of meshing phase separation between consecutive planets. That characteristic allows distinguishing different behaviours in the planets. Same behaviour occurs for planet-ring and sun-planet meshing. Nevertheless, this performance is clearly observed in the AE signals acquired with a fixed sensor due to the amplitude attenuation with distance. Figure 6 represents the signal pattern from the sequential meshing that allow us to distinguish main AE content from each pair of tooth. If load sharing variations were simultaneous the planets interactions would overlap in the AE signals.

One third of the gear mesh period corresponds, mainly, to each planet. This period can be divided in three sectors in which each planet is leading. It has been proved that no significant wave delay appeared because the short travelled distance. Therefore, the phase separation is maintained in the different planets activity. Three signals can be extracted for each planet by separating the three phase sectors (Fig. 7).

However, planet #1 activity is present in the rest of phase sectors when the separation is done. The AE events corresponding to planet #1, without surface treatment, are wider. Emission activity is longer in time, so they cannot be completely separated. Residual effect of planet #1 activity can be observed in planet #2 and planet #3 sector-signals. That wider event would be related with the roughness modifications due to the different surface finish.

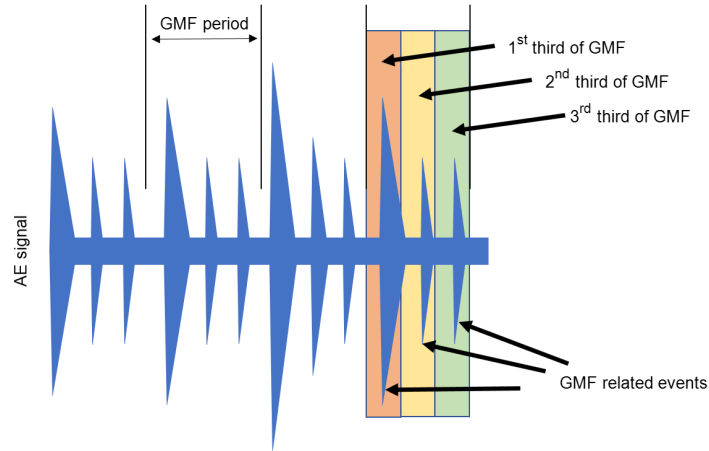


Figure 6: Scheme of AE events of sequential planet meshing and mesh phasing when a fixed AE sensor is used.

An incorrect meshing is performed because of errors in tooth profile geometry or because the incipient surface degradation.

Preliminary results obtained with planet #1 reveal a promising application for the study of these gears in such transmissions, due to the ability to distinguish the main signal content associated with each planet. Planet study makes it possible to relate the events observed in the AE signals to a given point of the meshing between teeth. As a consequence of the sequential meshing (ESSP transmission), events appear with a phase delay and can be identified because of the different attenuation, due to the variation in the distance between planets and sensor. Despite this, some aspects led to choose the sun as tested gear:

- Planet #1 degradation progression has advanced slowly. That happens because the system load is shared by the three planets. The complete load applied by the carrier is transmitted to the sun, one third of the load to each planet. Therefore, the expected degradation in the sun flanks is greater than the observed in the planet. Prior to the tests it is not known how fast the degradation will evolve.
- The planet is subjected to interaction with two elements, ring and sun. One tooth flank is always engaging with the sun and the opposite flank with the ring. Therefore, both flanks act in the load transfer. The wear

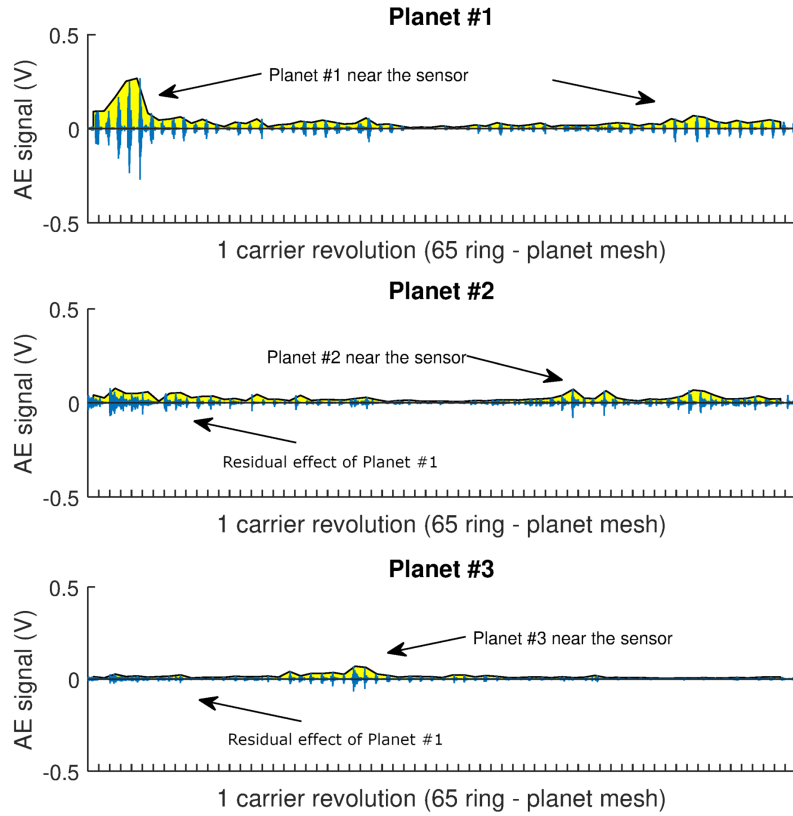


Figure 7: Separated signals (AE-fix sensor) corresponding to the main activity sector of one third meshing phase for each planet.

progression of both planet #1 flanks evolves simultaneously and in an heterogeneous way. This performance complicates an accurate analysis. On the contrary, the sun is only loaded on one active flank, allowing to correlate the sun active surfaces degradation with the degradation versus same components.

- The sun gear facilitates the mount and dismount operations to reproduce exact mounting conditions. Planets are mounted in the planet-carrier through bearings, tightened to their respective pin. Therefore, planet mounting conditions could be modified each test introducing uncertainty to the experiment.

The sun gear is therefore selected to perform the study developed in

following sections. The load is always applied in the same tooth flank (see the sun flank showed in Fig. 10). The wear originated during the degradation process is expected to appear in this active surfaces. Therefore, surface modifications can be directly correlated with the posterior signal analysis. Non-treated planet, or combination of non-treated gears, will be the subject of research in future studies.

3. Experimental set-up

The objective of the present study consists in the monitoring, by using AE signals, of the active surfaces degradation in a PG sun gear. To this end, a PG test bench was employed, emulating the operating conditions of a drive train wind turbine. The damage is induced to the sun by the PG operation under load with no seeded defects, only due to its interaction with the rest of gears. The PG transmission is actioned during a 9-test experiment according to operation conditions described in Figure 8.

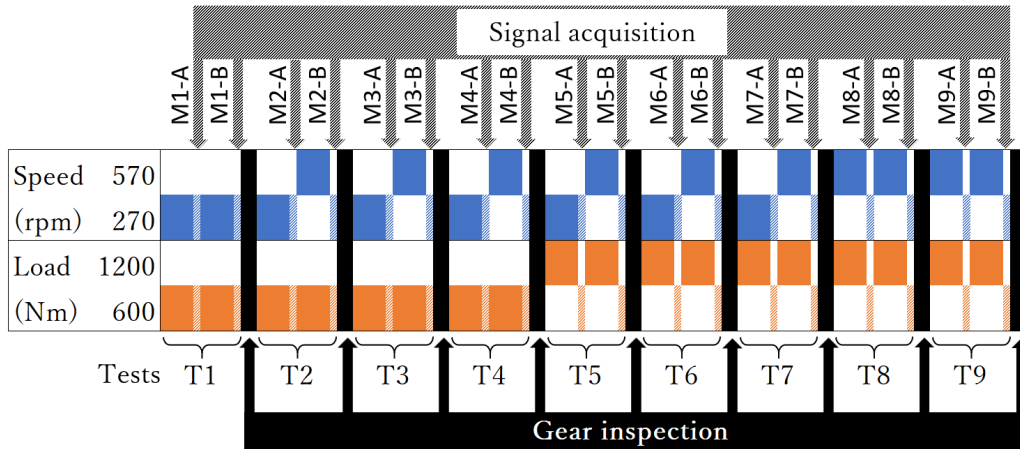


Figure 8: Test operation conditions.

The tests that constitute the experiment consist of the repetition of the following steps: transmission mounting, set-up, one-hour operation under load (signals are acquired during this interval), transmission dismount, gear inspection and cleaning. The procedure description is presented in Table 2.

Each test undergoes one-hour-work of the transmission under load, avoiding longer times without inspection. The method of oil lubrication is the oil bath, adequate for low-speed operation, that remains unmodified during this

Table 2: Test methodology.

Test stage	Description
Mounting and dismounting	The test bench must be dismantled and mounted again in the same position to perform the inspections.
Set-up and cleaning	After each test, the debris present in the lubrication oil (Ref. ISO VG 220) is cleaned in order to start the next test with clean oil and to control the degradation. The whole transmission stage is cleaned to avoid any particle: the gears are lubricated by its passing through an oil bath in the transmission bottom.
Operation under load	The test bench is operated during a one-hour time interval to control the damage progression. The load level is increased to maintain the degradation progress along the tests.
Gear inspection	<p>Gear visual inspection: Active surface modifications are monitored. Photos and annotations are used to compare the surface degradation in each test.</p> <p>Weight variation: The gear is weighed after being cleaned using a precision scale. The weigh variation enables to control the degradation process.</p> <p>Metallic debris control: Degradation process is shown and it can be induced from debris concentration and size.</p>

work time until its replacement before starting next test. Same oil volume is added each test to reach the centre of the rotating planets, lubricated by its immersion in the bath (Fig. 9). Initially, 270 rpm and 600 Nm are applied to the transmission (three masses are added to the load arm). Low speed and load help to avoid a premature degradation, keeping control of the surface wear. The only variation in these tests consists in a progressive increment both in load and speed, increasing in order to maintain the wearing progress during time.

The PG is monitored with AE sensors at both fixed and on-board positions (see Sec. 2.2). For the fixed position a magnetic holder is employed. On the other hand, on-board sensor is attached to the sun shaft with a holding device that incorporates a slip ring. The same volume of acoustic couplant gel is applied to each test in order to reproduce a reliable path for the AE signals.

As can be seen in Figure 8, the signal acquisition is performed at the

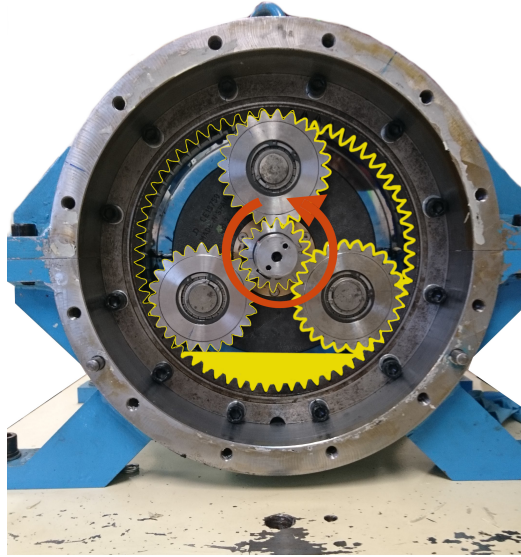


Figure 9: Scheme of the oil bath lubrication in the PG transmission.

middle (MX-A) and end (MX-B) of each test, at the same reference conditions of 270 rpm and 600 Nm. Where M means “measurement”, X is the test number and A & B are referred to the mid (A) or end (B) test time. This results into 18 measurements per sensor. In this work, two AE sensors and one accelerometer have been used, as presented in Sec. 2.2, making a total of 54 signals which are going to be presented along the results section.

The AE signal frequency content is characterized by the selected AE sensor. A VS150-RIC sensor (Vallen Systeme) is employed. With this sensor a good frequency response is obtained between 50 kHz and 600 kHz, showing the maximum response peak at 150 kHz where it exhibits a resonance. The AE sample rate is set in 2 MSamples/s, the maximum sampling frequency of the employed acquisition board (AD-Link USB-1210, 2 MHz per channel) and an acquisition time of 15 seconds per signal. This sample rate supposes that each acquisition needs 235 Mb of memory in the employed TDMS file format.

An uni-axial accelerometer Brüel&Kjær type 4398 is placed in parallel to the fixed AE sensor. The accelerometer is simultaneously acquired to the AE signals with a second acquisition board (NI USB-9162 with NI923).

4. Results and discussion

The different behaviours of sun active surfaces along the tests are correlated with the acquired signals to evaluate the AE sensitivity. First of all, the degradation process is described, pointing out the changes in the surfaces that influence the teeth engagement. Once the sun gear behaviour is established, an analysis is applied to the recorded signals. Finally, a condition indicator based on AE event width is proposed for active surfaces monitoring.

4.1. Overview of sun degradation and AE signals

Three degradation stages are recognizable during the physical inspection of the sun (Fig. 10). These stages involve three different contact conditions. Each stage is defined by a similar behaviour in terms of active surface state, roughness, damage, and material removal processes. Firstly, an extreme degradation involving material removal is observed (Fig. 10a). This first stage is followed by surface polishing and degradation stabilization (Fig. 10b). After that, pitting appears (Fig. 10c) and spreads along the surfaces (Fig. 10d and 10e). The details of these stages are described next and correlated with AE activity. A global description of each test can be observed in Table 3.

Table 3: Test parameters description.

Test num.	Weight var. (g)	Metallic debris in the oil (concentration / size / shape)	Surface damage	Degr. stage
1	-0.55	high / big / elongated and fine platelets	Material removal	1
2	-0.60	high / medium / elongated and fine platelets	Material removal	1
3	-0.03	low / small / principally fine platelets	Polished surface	2
4	-	low / small / principally fine platelets	Polished surface	2
5	-0.05	minor / small / fine platelets	Pitting appearance	3
6	-	minor / small / fine platelets	Pitting spreading	3
7	-0.03	minor / small / fine platelets	Pitting spreading	3
8	-0.01	minor / small / fine platelets	Pitting all flank	3
9	-0.03	minor / small / fine platelets	Pitting all flank	3

* The initial weight of the test gear was 400.91 g.

The test specimen, the sun gear without surface treatment, starts the experiments in manufacturing conditions and absence of defects. Soft parallel grooves originated by the cutting tool during its manufacture are the only rugosity observed in a magnified view. As normally happens, wearing process is expected till the perfect meshing is achieved.



Figure 10: Sun gear active surfaces photographed during the inspections at the end of the tests.

In the following, the description of the observed process is divided into the three phases involving different degradation conditions.

4.1.1. *First stage: extreme degradation*

Firstly, an extreme degradation process takes place during Tests 1 and 2, sharpen by the non-treated surfaces of the sun. The sun gear has lost mass up to 1 gram of metal during this period. The eroded material from sun surfaces appears as a high concentration of metallic debris immersed in the lubrication oil. A wide range of particle sizes is revealed in the debris

inspection, from small fine platelet-shaped particles (smaller than 0.5 mm) to metal needles about one quarter length of the gear width (Fig. 11).

The lubricating oil temperature is controlled measuring an oil sample extracted during the test. The temperature variation is shown in Fig. 12, representing the temperature evolution in the three degradation stages described above. The local temperature in the active surfaces is higher than the measured in the oil. Heat generated in the contact areas is transferred and dissipated to the oil and the rest of components. A remarkable increase in temperature is noticed during Test 1 (T1 in Fig. 12). It supposes a quick heat-transfer from hot metal surfaces to lubricating oil volume. External casing temperature is not been measured, but a significant overheating has been appreciated in the external PG casing only during the first two tests. Under this high stress and temperature behaviour, plastic deformation mechanisms could be accentuated in active surfaces. Abrasive wear mechanism takes place because of the hardness difference between treated and non-treated gear surfaces. The treated tooth penetrates the sun surface producing plastic deformations. Material is removed from the sun due to processes related with micro-ploughing and micro-cutting.

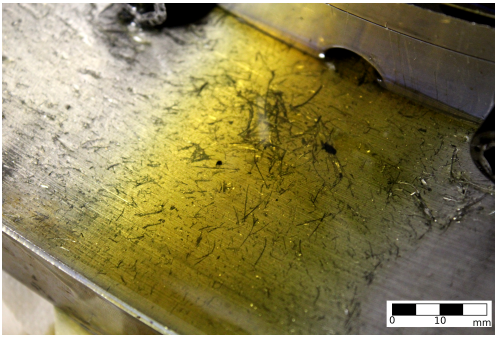


Figure 11: Metallic oil debris after Test 1.

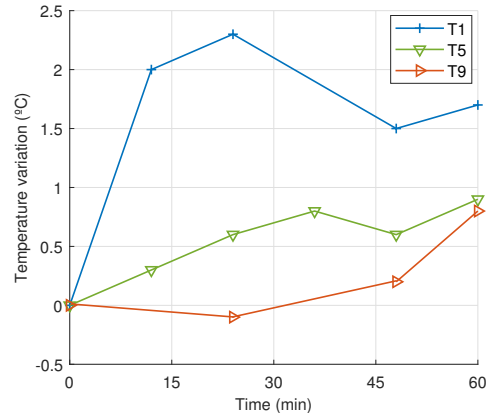


Figure 12: Oil temperature variation.

The needle-shaped debris allow to explain what happens during the gear mesh inside the PG in this first stage (Fig. 11). The material is teared away from the sun surface by sun-planet interactions. Planet teeth act as carving tools, removing material from the gear without surface treatment. The sun surfaces do not resist the drag stress and the material is removed in the sliding motion of the planet tooth. Thus, an incorrect gear mesh takes place due

to the material removal process. In normal conditions, the adequate teeth engagement follows a precise contact sequence. This sequence is composed by the motion transitions of sliding, pure rolling at the pitch point and sliding again in the opposite direction. Therefore, the high-pressure peak that should be achieved in the pure rolling condition is not reached [28]. High stress could be appearing in a longer section of the line of action instead to be concentrated in one point. Additionally, the load sharing would not coincide with the theoretically expected.

This extreme degradation process is clearly distinguishable in the AE signals, especially in the signals acquired with on-board sensor. The usual AE events related to the gear mesh show a sudden high amplitude burst followed by a quick attenuation, raising over the continuous base noise. However, this behaviour is not observed in parts of the signals during the extreme degradation process. The high amplitude burst is distributed in a wider time interval. A pattern without high amplitude peak is observed in some of the AE events during Tests 1 and 2 (Fig. 13). The AE energy release is not generated in a specific meshing point. A continuous high amplitude emission over the noise level is shown in these AE signals. This “wide event” shape would be related with the material removal. The high frequency bands are excited when the AE signal contains “wide events”. High AE intensity is displayed for 100 to 400 kilohertz range on AE signal spectrogram.

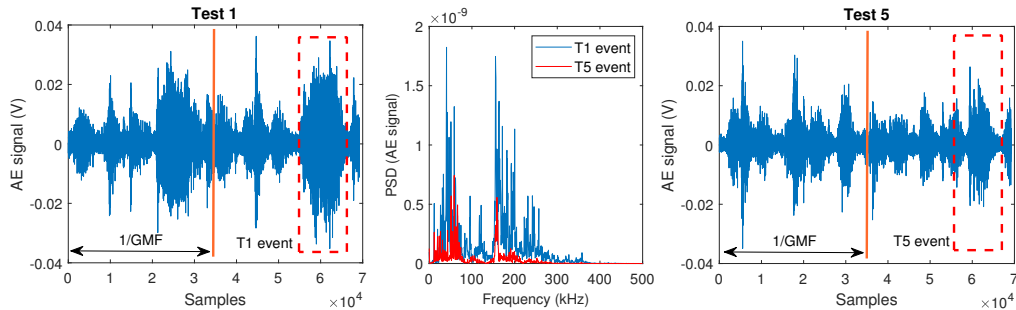


Figure 13: Time domain signal and spectrum of Test 1 and Test 5 events.

A parallelism with metal-polymer contact studies could shed light on AE monitoring when tearing away of wear particles is produced [29]. A relationship has been established between the event lifetime, or time width, and the magnitude and rate of solid destruction. The wear mass lost is correlated with an increase of the emission intensity for the total AE frequency range. Additionally, the separated wear particles that remain in the oil as debris will

act as punctual AE sources extended in the interaction between the contact surfaces. Therefore, the oil debris will be contributing to extend the event width.

In spite of the high debris concentration, the surface roughness is not especially affected by the particles immersed in the oil. The oil debris stuck between the engaging surfaces could provoke scratches or grooves in the sliding tooth direction [30]. In this first stage, no scratches in the sliding direction are identified in the visual inspection despite the big debris size present in the oil. The teared away particles come from the gear without surface hardening, this could explain the lack of scratches.

At the end of Test 2, an additional process to the material removal is shown. Sun active flanks are modified by the formation of hollowed areas because of the load sharing with planet teeth. The planet tooth footprints are stamped in the affected areas (Fig. 10a). This appears to be mechanisms of friction due to deformation and ploughing in spite of lubrication regime. Initially, the areas correspond to a small sector in the dedendum around the starting contact point. The footprint extension progresses along the sliding tooth direction, from the initial engagement in the dedendum until the end of tooth meshing at the tip. One side flank is mainly affected by the footprint, progressing in the flank direction, from left to right.

4.1.2. Second stage: footprints polishing

The second stage corresponds to Test 3 and 4. The corrected tooth surfaces led to an adequate motion transition in the gear mesh. The footprint area, observed in the sun flanks, results in an improved roughness. The footprint area is polished noticeably around the pitch point and along part of the flank during the meshing, showing a glossy appearance. Initially, only the left side of the planet footprint is affected, the same part where the footprints have started to appear. The polishing spreads progressively from initial flank areas to cover the entire width of active surfaces. It is not until Test 7 that the polished area reaches the whole tooth flank.

After the material removal, sun surfaces are adjusted to the shape of the planets. The deformation is dismissed and gear weight variation became stable. Less concentration of debris is observed in the lubrication oil. The oil debris became mainly fine platelets and the needles are not present anymore. Surface roughness is reduced after the first two test, showing some scratches in transversal direction (Fig. 10b), not related with he big size particles.

The absence of the extreme material removal in the sliding tooth move-

ment contributes to the sudden AE release. The wide AE events have already disappeared at Test 3, becoming sudden events. A different transition to dynamic friction is shown in the wide AE events. Both events display an increase of signal amplitude over the continuous AE activity when the teeth engage. In the case of wide events, this amplitude is maintained along the interaction period. A train of similar high amplitude waves is generated during this period. In regards to sudden events, as the events observed after the surface polishing, the initial amplitude raise is always followed by a train of high amplitude decreasing waves, reproducing a stick-slip AE activity [31].

The differences in the AE patterns can be explained as a result of the active surfaces interaction. When the material is being removed by the engaging in the sliding motion, the accumulated elastic energy would not be able to generate one sudden high amplitude event because of the material plasticity. The process of material removal, or the interaction with the removed particles, translates to continuous emission during teeth engaging. Dislocations interaction with obstacles is proposed as AE generation source in metal cutting process [32]. This dislocation emission mechanism works storing energy when the dislocation is close to the obstacle and releasing the energy when it is surpassed. Additionally, micro-cutting mechanisms could be affecting the AE generation in the abrupt debris tearing. Three-body abrasion due to the interaction of generated wear debris could take part in the continuous wider events. The complexity of this process makes it difficult to discern the AE source. Tribological experiments should be performed to analyse hard and soft gear tooth engaging, involving material removal, to better understand the process between the visual inspections performed at the end of each test.

4.1.3. Third stage: pitting

The third stage is characterized by the appearance of contact fatigue pitting during Test 5 (Fig. 10c). The system load is increased due to the degradation stagnation in the previous stage, which is observed in the visual inspection of gear surfaces, debris presence and weight variation (Table 3). Initial pitting scatters along the previously polished area. Thus, small disperse craters surge in the active flank. The pitting advances over the active surface, following the progression of the polished surface with a delay. The complete flank is affected at Test 7 (Fig. 10d), followed by the increase of the size and the concentration of craters (Fig. 10e). The highest point in pitting severity is reached during the last two tests.

The signals after Test 5 exhibit the same sudden AE events morphology as the ones observed after the surface polishing start (Fig. 13 comparing with Test 1 signals). Apparently, noisy signals and wider AE events are registered during this last part of experiments, coinciding with the pitting progression. The pitting progression in the sun gear is not directly interpreted in a signal overview description. The subtle modifications in the active surfaces due to the pitting, compared to the initial extreme degradation, need signal analysis to reveal the AE signals sensitivity.

4.2. AE signal analysis

AE signals from the on-board sensor located in the shaft are determined as the best source of information for the experimental process in the preliminary analysis (see Sec. 2.2). The main analysis performed in this article is carried out using on-board sensor signals because of its better sensitivity to the studied process, although, as described in Section 3, AE-fix and acceleration signals are also acquired during the tests.

To analyse these signals and to establish a correlation with the sun degradation, two main approaches are employed. Each one of them provides information of different aspects and entail a different difficulty in signal processing. First, a traditional CI analysis (RMS and kurtosis) provides low-requirement processing suitable for AE. Secondly, the spectral content is analysed, which in the case of the AE signal involves working with large signals. The frequency study includes the raw and envelope AE signal, which is useful to establish a proper comparison with the acceleration signals. Finally, in order to obtain representative information by means of algorithms that enable data reduction, a new CI is established in the following section based on the stated results.

Moreover, the study of the process sensitivity from external fixed sensor position is evaluated. A comparison between AE and vibrations technologies is performed using these fixed sensors. Vibration analysis using accelerometers is a widely employed monitoring technology, but it presents lack of sensitivity in certain specific performances, as low-speed regimes in the case of rotating machinery [30]. AE is postulated as an alternative technology in these cases due to the acoustic perturbations generated by the surface interaction of tribological contact. Different physical mechanisms are involved in AE generation, achieving to register malfunction by slight magnitude perturbations produced by subtle changes over the teeth surfaces, neglected by vibrations. For example, it has been observed that AE provides better fault

indicators than vibrations in subtle situations because of its insensitivity to mechanical background noise [33].

The global evolution of the experiments is analysed using traditional CIs as RMS, kurtosis, crest factor or counts number. The three degradation stages mentioned above are not clearly distinguished by different tendencies in the signal characteristics through these CIs. Figure 14 shows the averaged RMS and kurtosis value for each test.

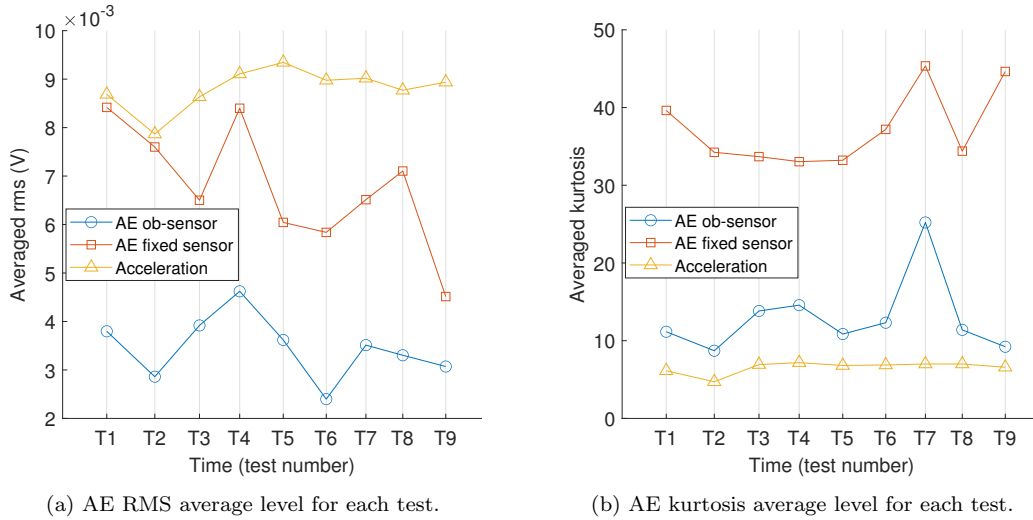


Figure 14: Indicators from the AE and acceleration signals, acquired at the reference operating conditions (270 rpm and 600 Nm).

Nevertheless, the process description is neglected in the CIs evolution for all the used sensors: on-board AE sensor, fixed AE sensor and fixed accelerometer. In spite of that, the RMS describes a decreasing tendency from the fixed AE sensor signal (Fig. 14a). That is, the initial values are higher and decrease with the progression of the tests. This progression is consistent with the improvement of the meshing conditions but obviating the pitting progression. Therefore, the initial sun fitting progression can be observed by using the external fixed AE sensor, as an indirect effect of the degradation. Nonetheless, results reveals that AE RMS or kurtosis would not be the most appropriate CI. This observation does not imply a sensitivity to subtle sun surface variations. However, same CIs calculated from acceleration signal, with the sensor placed in the same position than AE fixed sensor, offer a flat response.

A linear relationship between the increase of pitting rate and the AE RMS has been observed in spur gears [16]. The fluctuating values in the on-board AE sensor signals are especially unrepresentative about pitting progression. The simultaneous processes of polishing, erosion and pitting makes it difficult to observe any descriptive tendency between Test 2 and 6. However, it is noticed that the RMS in on-board signals decreases from Test 7 to Test 9, a period where the pitting is the main process and its severity is highlighted. Tribological studies have shown an AE RMS reduction in late micropitting stages due to the surface softening [34].

Regarding the evolution of the signals acquired in one specific test, an RMS increasing tendency is observed in the on-board sensor signals. Signals recorded under the same operating conditions of load and speed present a slight and progressive RMS increment, reaching its maximum at the end of the experiments. The debris immersed in the oil could be related with this progressive RMS increment [35]. The accumulation of degradation debris between the engaging surfaces would increase the released AE. At the beginning of each test, clean oil is added after cleaning all components. After that, the tests are carried in continuous operation without dismounting, elevating the concentration of oil debris.

Given the fact that the focus is on studying the influence of subtle phenomena in the PG behaviour, a traditional CI monitoring approach is not the most suitable strategy. The influence of all operation parameters, such as the effect of the debris immersed in the lubricant, could be reflected in AE signals with similar magnitude than the effects of the monitored process [36]. An identification of the signal generated in the moment of active surfaces interaction can provide useful CIs. A recent study has revealed a correlation between a modified RMS indicator and the pitting area [20]. In that study, where an ordinary transmission is used, the indicators are expressed in terms of gear mesh cyclostationarity. A correlation between the active surface in contact and the AE activity generated at that moment is achieved. AE events morphology is related with the contact area in each meshing point. However, in a PG, with multiple overlapped AE sources, to express the AE signal versus gear roll angle is complex.

Spectral analysis of raw AE signals allows to evaluate its frequency content, correlating the intensity of peaks or frequency bandwidths with operational conditions. The process evolution expressed through the sequence of signal spectrum does not show a precise description of the degradation process. As above mentioned for signal RMS, on-board signal spectra ex-

hibits fluctuating values in its amplitude. For the AE fixed sensor signals, a spectral area reduction along the experiment is observed, reproducing the RMS tendency (Fig. 15).

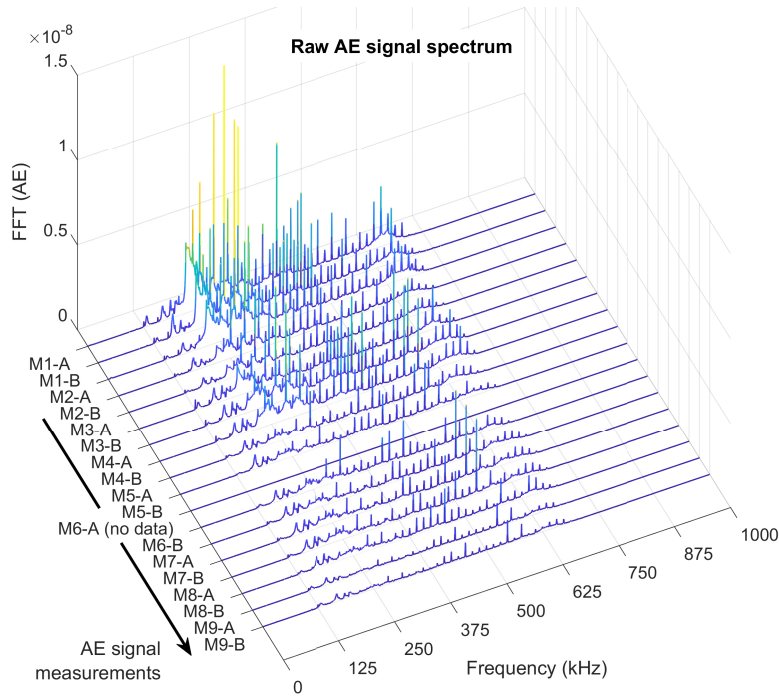


Figure 15: PSD evolution of fixed sensor AE signals during the tests.

Spectrum variations happen globally, consequently, no frequency bands show a specific response to tests evolution. For the interpretation of the fixed sensor signals, the influence of oil debris should be especially mentioned. The metallic debris ends in the lubrication bath located in the gearbox bottom covering the ring gear, particularly affecting ring-planet engaging. Lubricant conditions have been pointed out determinant in AE amplitude and frequency spectrum in PG monitoring using an external sensor [12].

To obtain the frequency information of the gear mesh periodic signals an envelope analysis is performed. The downgrading of high sample rate signals to low frequencies allows to express the spectral content in terms of the frequencies of interacting components (shaft, carrier, gear, ...). AE envelope spectra analysis is performed using Hilbert transform from raw AE signals.

AE envelope spectrum from the on-board sensor signals is displayed in Fig. 16. The GMF is displayed in every test signals. Two recognizable sidebands around the GMF are separated by a frequency length of $GMF/2$.

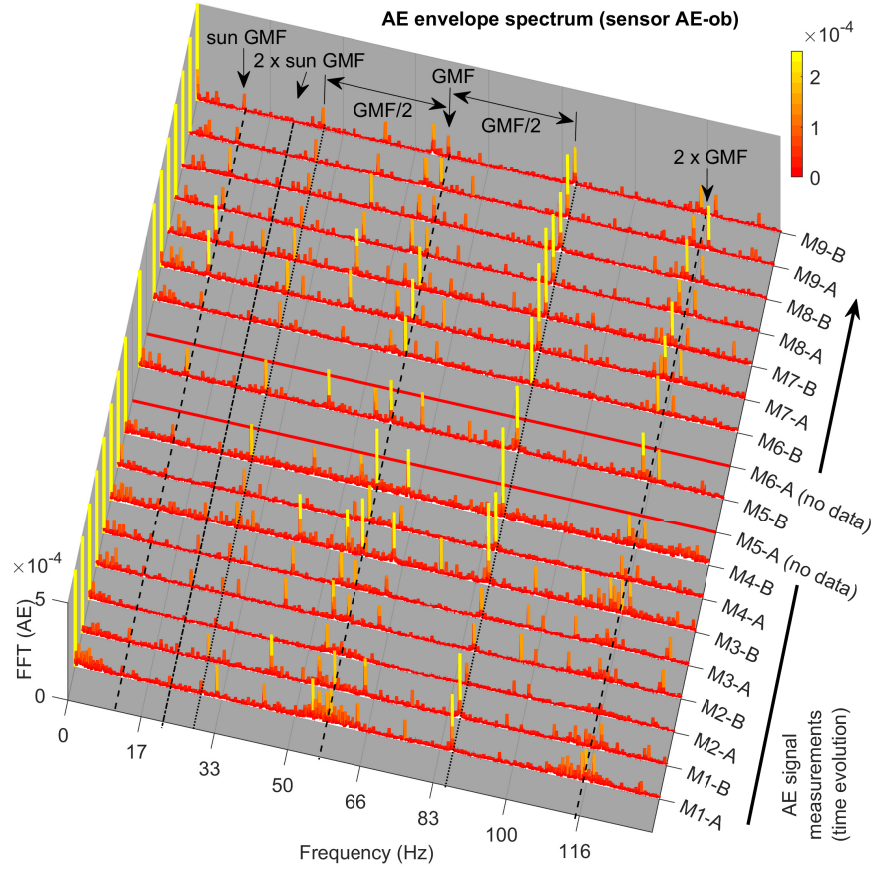


Figure 16: AE envelope spectrum from on-board signals (this figure is intentionally cut in the z axis because of display purposes).

For the first tests, the sidebands are not clearly distinguishable from GMF peak because of the noisy AE signals. The amplitude of the upper one, frequency $GMF + GMF/2$, is increased in the last stage of the tests. This sideband is close to a harmonic of the sun fault gear mesh frequency (f_S in this article “sun-GMF”, see Appendix A.3). The envelope spectrum sequence of on-board signals is mainly affected by f_S , the sun fault frequency (Eq. A.7), and its harmonics.

In regards to the AE envelope spectrum results in the on-board sensor,

the sun-GMF exhibits low amplitude during the first tests. This frequency content raise its spectral level after Test 3 as seen in Fig. 16. However, this initial lower level is not repeated by the sun frequency harmonics. In spite of the noisy signals, sun-GMF harmonics are observable since the beginning of the experiment, maintaining a peak amplitude throughout of the tests. After Test 3, envelope spectrum becomes less noisy, coinciding with the tooth roughness improvement. Therefore, a clearly defined GMF peak is exhibited. The variations observed in the envelope spectrum along the tests progression reveals modifications in the gear mesh.

On the other hand, the sun-GMF is not visible in the AE envelope spectrum of the fixed sensor signal (Fig. 17). In the envelope spectrum of the AE fixed sensor, the GMF and the planet carrier frequency (the frequency associated to the rotation of the planet-carrier) are the main components.

The amplitude modulation, due to the relative movement between planet and sensor, is expressed as two sidebands above and below the GMF. These sidebands are separated by the planet carrier frequency, $GMF \pm \text{carrier frequency}$. A higher peak amplitude is shown during the first two tests in the envelope spectrum. However, no significant change is noticeable in contribution of the different peak frequencies along the degradation progression.

The acceleration spectrum evolution (Fig. 18) reveals the sun-GMF peak but not at the beginning of the experiments. A distinguishable peak can be observed in the signals of the second half of the experiment, after Test 5. In spite of the peaks presence, no tendency is followed by their amplitude with the degradation progression. The sun-GMF peaks appear in the period related with the pitting spread. However, acceleration spectrum is less perturbed at first tests, showing a similar behaviour despite the initial extreme material removal.

The fixed sensor envelope spectrum can be compared with the acceleration spectrum placed side by side with this AE sensor in the PG casing (AE fixed sensor position, see Fig. 2). Both sensors have been receiving same perturbation waves but the response to the initial degradation stage is completely different. Meanwhile the acceleration is measured as the perturbation of a seismic mass, the AE sensor transforms the waves direct effect over the piezoelectric crystal. AE envelope and vibrations signal are not equivalent.

Both CIs and frequency analysis do not present a clear trend about what happened during degradation. In particular, the spectral study of the signals, which involves greater detail and more advanced processing, does not show evidence of being the optimal approach for the analysis. Because of this, the

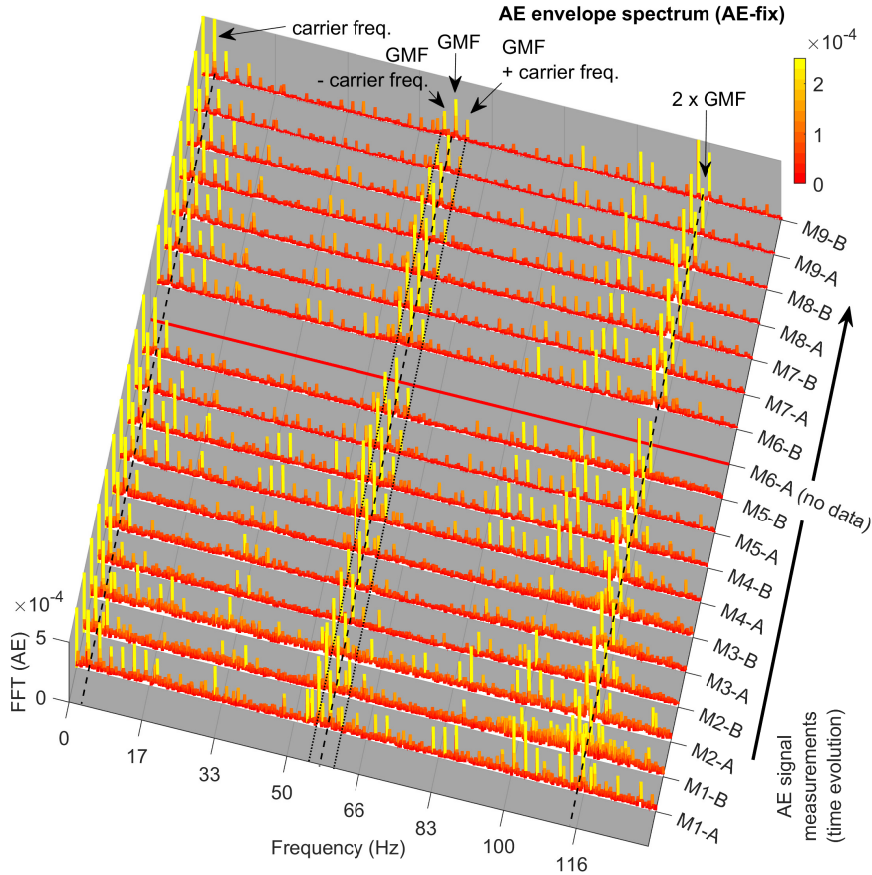


Figure 17: AE envelope spectrum from fixed sensor signals (this figure is intentionally cut in the z axis because of display purposes).

authors have proceed to develop an indicator that reflects the changes that occur in the signals.

4.3. Event width as damage indicator

In the previous description of the signals, a wider AE event is detected as indicator of the gear degradation process. Variations in the event pattern of the time domain signal reveal an incorrect contact between gears. Regarding this behaviour, the AE lifetime or event width could be a useful property to evaluate the gear active surface monitoring.

The AE event width can be detected by using a threshold crossing algorithm. One event is represented by three values related with the signal

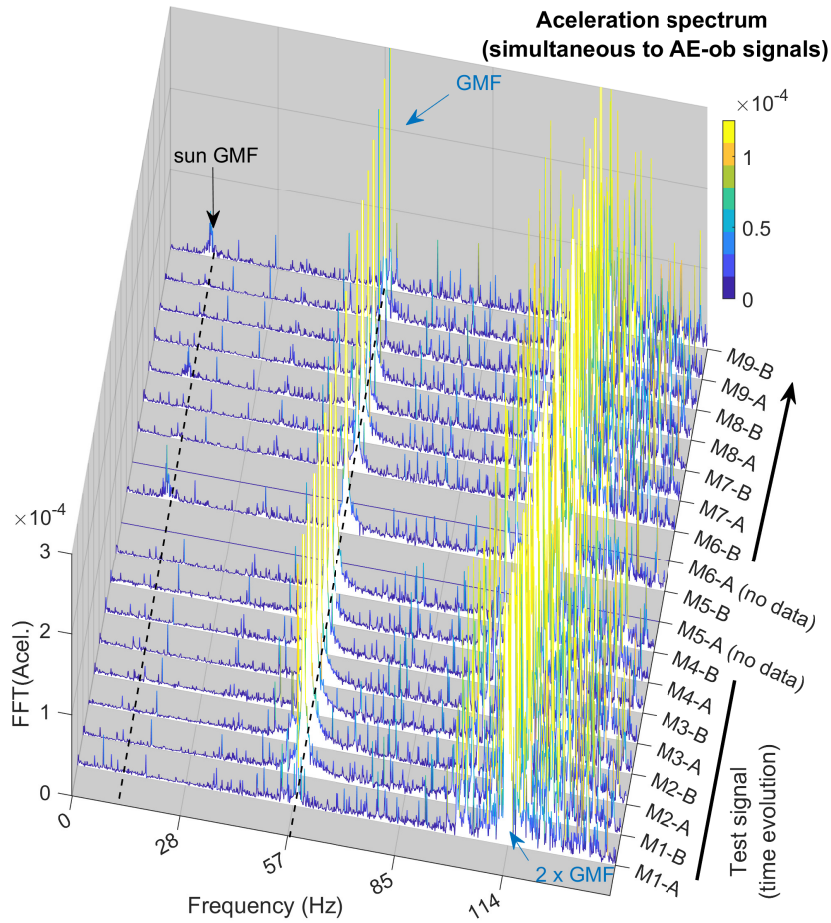


Figure 18: Acceleration signal spectrum (this figure is intentionally cut in the z axis because of display purposes).

breaking of the threshold: rising time, maximum value time and descending time. This methodology is based in a previous work [37] where a method is defined for data reduction in AE signals consisting of a triangular signal. A new signal describing the gear mesh related events is derived from the raw signal reducing dramatically the data. For the present study, only the rising and descending times are considered. One “event width” value is calculated for each signal by averaging all the detected events.

A correct threshold setting is the most critical point in any event detection algorithms. A fixed value or an automatic threshold based in the acquired data can be employed. Both possibilities are evaluated in the present study.

A preliminary analysis of every signal shows that the continuous AE noise level is maintained along the same test signals. Therefore, one fixed voltage level was selected to represent the event detection for each one of the nine tests. A frequency domain analysis of the discrete signal is performed using Lomb periodogram to check the selected threshold effectiveness. The frequency peaks observed in the discrete signal spectrum coincide with the raw AE envelope spectrum assuring the relation of the detected events with gears engaging.

The progression of this event width value and the weight variation are shown in Fig. 19. The initial extreme degradation process is expressed by the highest indicator values in the two first tests. This indicator is reduced after Test 3, showing the improved meshing conditions after the gear weight stabilization. First part of the experiment is reproduced by the averaged indicator values, but the pitting progression is not expressed.

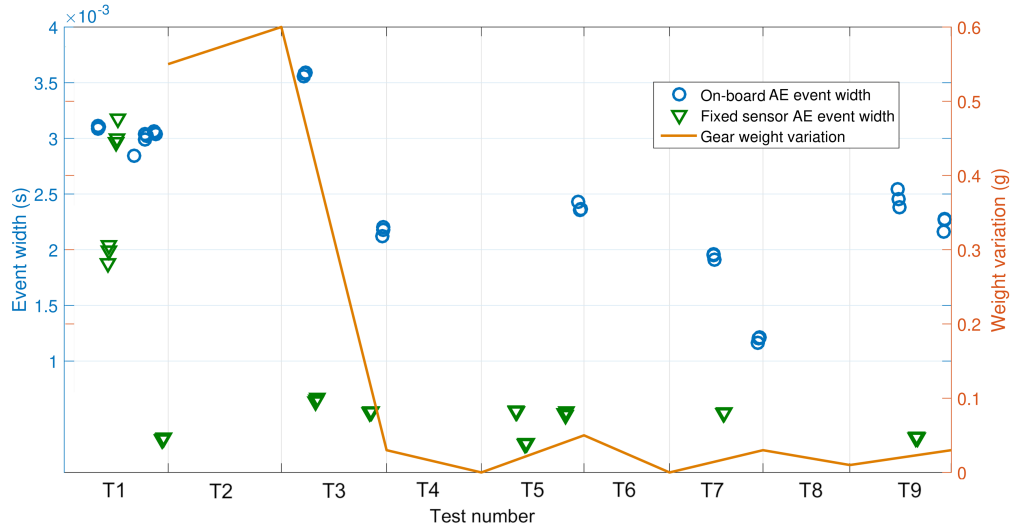


Figure 19: Example of averaged peak width evolution considering just the bursts overpassing the mean level considering every signal from odd tests (AE-ob, 270 rpm and 600 Nm).

The previous analysis can be enhanced considering the PG periodicity and gearbox configuration in the event width evaluation. A CI with these assumptions, denoted as event width indicator (EWI), is developed. The EWI expresses a characteristic value by estimating an event width related with the monitored gear (Fig. 20).

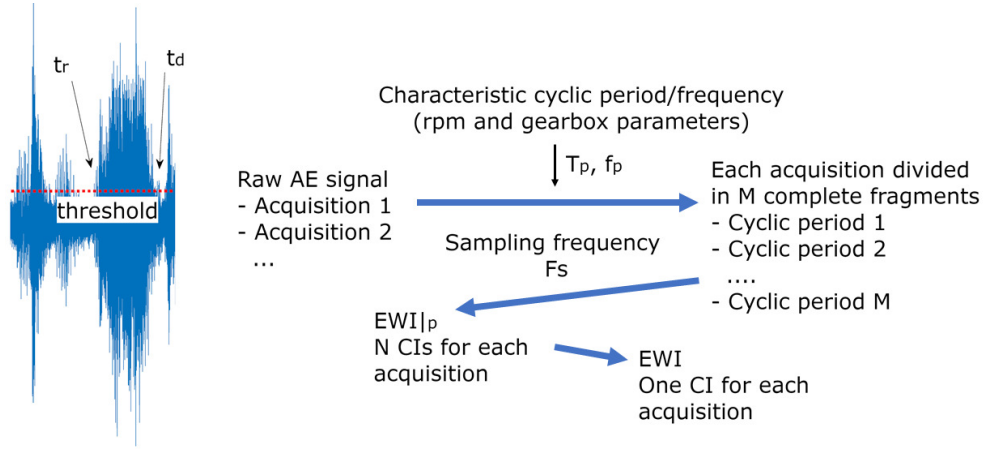


Figure 20: Scheme of the EWI calculation.

First of all, a cyclic interval of interest for the gear is selected. The number of expected events N , or number of teeth engagements in that interval, T_p , is already known. AE signals exhibit numerous events, some of them can not be attributed to specific phenomena due to its random nature. Nevertheless, the engagement events are, in general, distinguished from other components interaction or random events because of its superior amplitude and lifetime. As mentioned above, the “sun cycle” is the relevant period for the monitoring of the sun active surfaces (see Appendix A.2). The number of the expected widest events in each defined interval corresponds to the sun number of teeth, $N = Z_S$.

Each one of these N events are identified by the crossing of an amplitude threshold. The width of the event is simply defined as the difference between the rising time (t_r) and the descending time (t_d) over the threshold. The event width for one p period is represented as the average of the N values (Eq. 2).

$$EWI |_p = \sum_{i=1}^N \frac{(t_r^i - t_d^i)}{N} \text{ for } i = 1, 2, \dots, N \quad (2)$$

Finally, more than one period are evaluated to obtain a characteristic value, avoiding random fluctuations. The EWI is calculated as the averaged value of the integer number of the defined period inside that signal, $M = \lfloor t/T_p \rfloor$, being t the duration of the entire signal (Eq. 3).

$$EWI = \frac{1}{m} \sum_p^m EWI |_p \text{ for } p = 1, 2, \dots, M \quad (3)$$

As the degradation is homogeneously distributed along the gear teeth the averaged value provides a representative value of the global surface behaviour. However, local defects in one tooth could be identified dividing the period in teeth sectors.

An automatic threshold setting is defined for the EWI calculation based in each window RMS level. Threshold optimal selection requires iterative analysis until an accurate identification is achieved. A small variation is observed in the ratio between peak amplitude and the continuous emissions level when the cyclic period is evaluated. Therefore, the automatic threshold is accurate for the short and repetitive signal fragments. Furthermore, the dispersion of the EWI period values ($EWI |_p$) is reduced when the representative cyclic period is applied. This methodology can be used in on-line AE signal processing or using the recorded signals. Additionally, the rotation speed can be estimated through the GMF extracted by the AE envelope analysis, without needing extra instrumentation to implement the monitoring.

Three EWI levels are obtained, representing the three degradation stages observed during the tests (Fig. 21). In Figure 21, signals are acquired with AE-ob sensor at the same operational conditions, varying only the surface status due to the degradation between successive measurements. Test 1 and 2 stand out over the rests, as it happens in the results obtained with the simplified average because of the evident bigger events. Second stage is shown as a reduction of the EWI value. This reduction of the burst width coincides with the polishing of the contact surfaces, without a severe progression of the incipient pitting. Nevertheless, last tests, 8 and 9, are discerned by a higher EWI value. The identification of the pitting final stage, is represented with this indicator. However, the variation is less subtle than for the first stage due to the less severe modification.

The debris presence in the oil can affect the values of EWI owing to the modification of the contact behaviour because third body interaction. This is due to the initial low debris content because of the cleaning of the gearbox after the previous test. Therefore, fluctuations in EWI values within one test can be attributed to this aspect that modifies apparent similar operational conditions. Lower EWI values are obtained at the beginning of each test, as mentioned above for the RMS evolution (in Section 4.2).

This progression depending on the test time is shown in Fig. 22, where

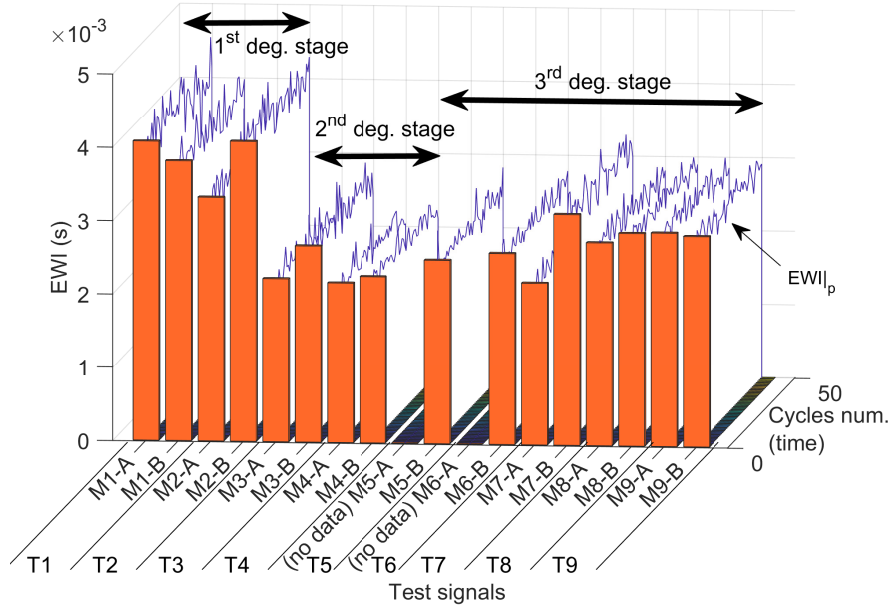


Figure 21: EWI values along the tests from AE-ob sensor at reference conditions (270 rpm and 600 Nm).

mid-time-signal (MX-A) and end-time-signals (MX-B) evolution are separated (same values than Fig. 21). Signals at mid test (MX-A measurements) correspond to cleaner oil than signals at the end of each test (MX-B measurements). EWI in Test 1 and 2 displays a reduction from M1-A to M3-A, coinciding with the diminution in the degradation severity, and an increment in the last part from M7-A to M9-A after a stagnation. On the other hand, MX-B measurements are significantly affected by the presence of debris. A decrease in EWI value is observed from M2-B to M3-B, distinguishing the two stages. A slight but progressive increment appears from M5-B to M7-B, at same time that pitting progresses. Finally, EWI value is reduced in M8-B and M9-B when the final pitting stage.

Figure 23 represents together the CIs studied in this work, including RMS, kurtosis and EWI. CIs values are normalised with respect to their maximum value (0.0093 RMS values, 45.3523 for kurtosis values and EWI 0.0039), in order to be able to compare them.

According to the CIs evolution, in Fig. 23 there is a decrease in EWI value from Test 2 to Test 3, which indicates the different degradation conditions between first and second stage. The rest of CIs reduce their value from Test

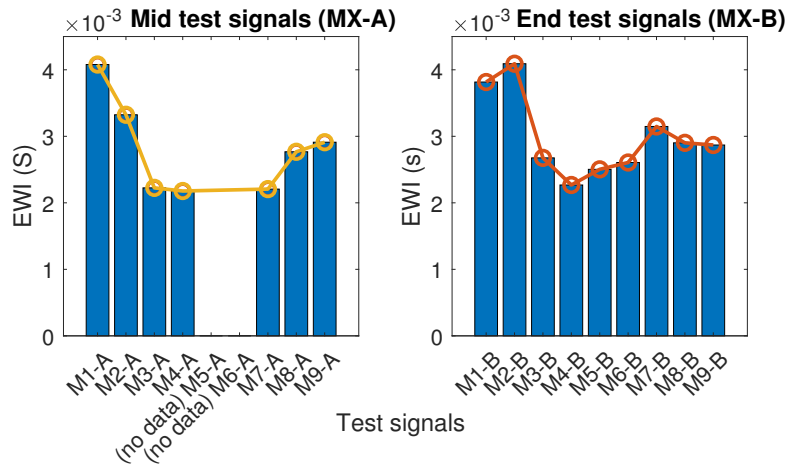


Figure 22: EWI values along the tests separating mid-time and end-time measurements.

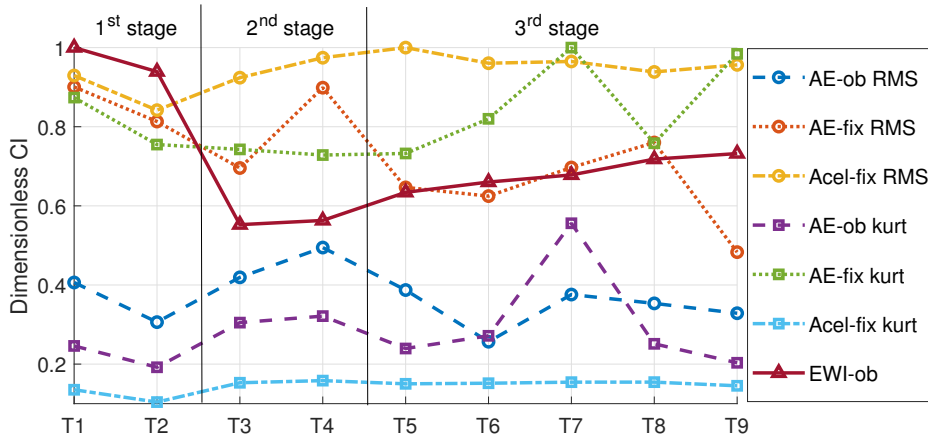


Figure 23: Averaged value of the studied CIs (dimensionless) along the tests.

1 to 2, as an improvement of the meshing conditions from the initial wear. Nevertheless, the transition to second stage supposes a slight modification in the tendencies of non-EWI CIs. Second stage reveals a growing tendency in the AE-ob RMS, Acel-fix RMS, AE-ob kurt and Acel-fix kurt. AE-fix RMS and AE-fix kurt show a stable and fluctuating tendency respectively during second stage. The averaged values of EWI rise progressively after Test 4 representing third degradation stage. The rest of CIs show different trends depending on the employed sensor during the third stage. Acceleration from Acel-fix RMS exhibits a slight reduction, shared by AE-ob RMS after Test

7. AE-fix RMS reproduces a fluctuating descending tendency, meanwhile AE-fix kurt is ascending. In conclusion, the CIs can be correlated with certain aspects along the degradation progress. However, according to their evolution and the magnitude of the changes, the EWI displays the most suitable tendency to the degradation progression.

5. Conclusions

The generalization of correlations between operational parameters, e.g. speed or lubrication regime, and AE signal values, as RMS, in a complex system as a PG needs certain monitoring set-up considerations. Sensor position, acquisition time target or cyclic periods performed by the components, are important factors that must be specifically assessed for the monitored specimen. Therefore, subtle phenomena during the contact process between surfaces can be observed or ignored depending on the main source of the waves arriving to the sensor.

The experimental work using a PG reproduces different active surface behaviours along the gear degradation process, boosted by the absence of surface treatment, that are reflected in AE signals. Through the adequate sensor emplacement in the sun shaft, the sun-planet meshing is displayed as AE burst events in the acquired signals. Therefore, the conditions of the contact sequence and the surface roughness can be studied regarding these events, in particular with the emission lifetime or activity width of these events. Thus, it is proved that AE can be used for the monitoring of the active surfaces of a specific PG component.

Signals acquired under the degradation process of active surface material removal have shown the absence of a single sudden high intensity release of energy in the AE burst, linked with the absence of a correct contact sequence. On the contrary, this wide AE event is recorded as a wide emission with continuous high amplitude. The oil debris presence between contact surfaces and the different contact mechanisms in this unusual condition are remarked in the results discussion. On the other hand, the active surface polishing is observed as well-defined AE events and pitting spreading as a subtle deterioration of this aspect.

Finally, a CI denoted Event Width Indicator (EWI) is developed based on the AE event width or emission lifetime. The correlations between global operational parameters and AE CIs, such as RMS or kurtosis, are unsuccessful to express the surface behaviour. Nevertheless, satisfactory results

are obtained when an average of the EWI is performed with respect to the cyclic meshing period of sun surfaces, reflecting the importance of the considerations mentioned above for the experimental set-up. EWI-ob seems to reflect the stages of physical degradation, proving to be a promising alternative to other indicators. Other sensor positioning, different than the sun shaft, has failed to express the sun active surfaces behaviour. Only subtle indirect effects of the degradation process can be observed in an external case positioning, employing an AE sensor and a parallel installed accelerometer by means of frequency analysis.

Acknowledgements

This work was supported by the Spanish Ministry of Science, Innovation and Universities (MICIU) [project DPI2017-85390-P]; SODERCAN under the call ‘R&D in marine renewable power’ [RM16-XX012]; and the Spanish Ministry of Science and Innovation (MICINN) [PID 2020-116213RB-I00].

Appendix A. Fundamentals and considerations

The monitoring of PG with AE requires to understand certain characteristics that are critical for the application of a correct strategy. This is the reason why, in order to perform the correct experimental set-up, some specific aspects about PG and AE had to be studied such as the mesh phasing, mesh cycles and mesh frequency. The fundamentals of these aspects are presented in the following sections.

Appendix A.1. Mesh phasing: sequential or simultaneous

The mesh phasing depends on the PG geometry, affecting the dynamic behaviour of planetary transmissions. Depending on this parameter, the load sharing among gears is produced simultaneously or with a phase delay between planets. If the planets have the same geometry, the gear mesh behaviour is exactly repeated in the interaction of each planet with ring and sun. Therefore, the only variation regarding the mesh phasing is the synchronicity of the planets meshing performance.

A PG can be classified in terms of mesh phasing according to the relationship between two of its geometrical parameters, the ring number of teeth (Z_r) and the planet angular spacing (ψ_i) [23]. The planet angular spacing, ψ_i , is defined as the separation angle of the i planet-carrier pin, where planets

are mounted. Depending on whether the equation A.1 is fulfilled or not, the phase behaviour is established.

$$\frac{Z_r \psi_i}{2\pi} = n \quad (\text{A.1})$$

Where the index i refers to each planet ($\psi_i = \psi$ if all planets are equispaced) but n must be an integer number.

In-phase In this kind of transmissions, each planet meshing corresponds to the same point along the line of action. That means that the interactions between gears are simultaneously produced in all planets, therefore the pitch point and the contacts happen at same time. An in-phase PG must fulfil the Eq. A.1.

Sequential phase Each planet meshing corresponds to a different point along the line of action, existing a meshing phase separation between consecutive planets of one divided by the number of planets. In a sequentially phased PG, the pitch point contact is reached at a different time in each planet, but with equal delay between them. Eq. A.1 is not fulfilled and the planet angular spacing (ψ_i) is the same for all planets.

Arbitrary phase In case of the planets are not equally spaced along the planet carrier, an additional classification can be identified. In an arbitrary phased PG each planet meshing corresponds to a different point along the line of action without the same phase between planets. The gears behaviour is not in-phase and the phase distance between planets depends on the PG geometry. Eq. A.1 is not fulfilled and the planet angular spacing (ψ_i) varies.

Appendix A.2. PG mesh cycles

In the PG, its components repeat periodically their positions in the relative movement among planets, carrier, sun and ring. For example, the planets centres repeat their azimuth position with respect to the ring every carrier revolution. Although this cycle is completed, the teeth surfaces in contact will normally be different because the planets rotate around their axis. Therefore, several cycles that have different effect in PG performance can be defined. These cycles duration can be calculated in terms of shaft revolutions by expressing the relations between the components angular speeds (Eq. A.2 and A.3).

$$\begin{aligned}\dot{\theta}_{S/0} &= \dot{\theta}_{C/0} \left(\frac{Z_R}{Z_S} + 1 \right) \\ \dot{\theta}_{P/0} &= \dot{\theta}_{C/0} \left(1 - \frac{Z_R}{Z_P} \right)\end{aligned}\tag{A.2}$$

$$\begin{aligned}\dot{\theta}_{P/C} &= -\dot{\theta}_{S/C} \frac{Z_S}{Z_P} \\ \dot{\theta}_{P/C} &= \dot{\theta}_{R/C} \frac{Z_R}{Z_P}\end{aligned}\tag{A.3}$$

Where $\dot{\theta}$ is the angular speed and the subscripts express the components in relative motion, being the 0 subscript the reference system fixed to the ground and C to planet carrier holding element. Z expresses the number of teeth and the sub index S, P, R refer to the sun, planet and ring gears respectively.

If the ring is the fixed gear, its angular speed is equal to zero (Eq. A.4).

$$\dot{\theta}_{R/C} + \dot{\theta}_{C/0} = \dot{\theta}_{R/0} = 0\tag{A.4}$$

Thus, the previous equations can be written as Eq. A.5:

$$\begin{aligned}\dot{\theta}_S &= \dot{\theta}_C \left(\frac{Z_R}{Z_S} + 1 \right) \\ \dot{\theta}_P &= \dot{\theta}_C \left(1 - \frac{Z_R}{Z_P} \right)\end{aligned}\tag{A.5}$$

Three cycles are defined in this paper:

Complete PG cycle After this period is completed, the position of all the elements is repeated exactly. The planets rotate over their central axis at the same time than the carrier rotates around the sun; therefore, several shaft revolutions are needed to repeat same pair of gear flanks interaction. The number of revolutions for a fixed ring PG is obtained by expressing the relation between the input angular speed $\dot{\theta}_S$ and the output $\dot{\theta}_C$ (Eq. A.5).

Carrier cycle It corresponds to one planet-carrier revolution. The carrier cycle is relevant for the understanding of the obtained signals. The

mass distribution is repeated with every carrier rotation and, consequently, the planet center azimuthal movement. The system load sharing exhibits a periodicity in this cycle. However, the active surfaces in contact do not have a periodic behaviour in this cycle. The duration of the carrier cycle can be directly expressed in terms of sun shaft revolutions using the transmission ratio in the test rig.

Sun cycle A sun cycle is completed when each one of sun active surfaces have engaged, with any of the planets. Therefore, every active flank of the sun has interacted but not all planet teeth have engaged during this cycle. If the damage is focused in the sun active surfaces and planets remain in good conditions, this cycle can be valid to detect defects appearing in the sun flanks.

The period for the “complete PG cycle”, that repeats every active surface interaction, could require a technically-non-affordable duration with high acquisition rate signals due to the resulting file size. Hence the convenience to define cycles, smaller than the complete one, that can be used as alternative for monitoring in order not to dismiss relevant events.

Appendix A.3. PG mesh frequencies

The gears engage periodically repeating the meshing at a certain frequency. Beyond its mesh phasing, the PG gears mesh at a certain frequency. This gear mesh frequency (GMF) is derived from the gears number of teeth and the rotational speed. Besides the GMF, other frequencies can be defined in a PG in relation with appearance of faults or defects in the gears, for example, the frequency of a single tooth meshing [24]. These frequencies are employed for the signal analysis, allowing the interpretation of the frequency spectrum. Two mesh frequencies are used in this paper:

GMF The Gear Mesh Frequency expresses the periodicity of teeth gears engagement. GMF can be calculated with the rotation speed and the number of teeth. Eq. A.6 shows the GMF for a PG.

$$GMF = \frac{n_1 Z_S Z_R}{60(Z_S + Z_R)} \quad (\text{A.6})$$

where n_1 is the sun shaft rotation speed in rpm and Z is the number of teeth, for the sun (Z_S) and ring (Z_R) gears.

Sun-GMF The sun-GMF corresponds to the mesh frequency of a local defect in a sun tooth, as describes Eq. A.7.

$$f_S = \frac{n_1 N_P Z_R}{60(Z_S + Z_R)} \quad (\text{A.7})$$

In Eq. A.7, f_S is the “sun-GMF”, N_P is the number of planets, n_1 is the sun shaft rotation speed in rpm and Z is the number of teeth, for the sun (Z_S) and ring (Z_R) gears.

Appendix A.4. Acoustic Emission technique

AE signals are acquired using a high sample rate (Megahertz range). This is due to the high frequency information about sudden pressure variations from multiple sources that is carried by the acoustic waves. Therefore, millions of samples per second are recorded to obtain representative signals with AE sensors. The high bandwidth is a key in the sensitivity of this technique. However, this high frequency generates big size files, making difficult the computational handle of the data and its storage during long time monitoring periods. This computational limitation suggests to set a minimum signal duration in order to work with the recorded files.

The signature of a mechanical system can be obtained through AE by the acquisition of several signals during its operation conditions. Nevertheless, it is not just a matter of the biggest number of possible measurements. If the process is not stationary, as happens in geared transmissions, the minimum acquisition time must be set in order to record all interactions during machine operation cycle. For example, in a simple gearbox with two gears, one revolution of the biggest gear is enough to assure every contact acquisition. Otherwise, a single local defect could be always ignored.

The relative movement of the components in PG or in a machine with several transmission stages suggest a longer time of acquisition than simple mechanisms. Therefore, the “complete PG cycle” could not be technically affordable for a monitoring strategy with high acquisition rate signals due to the resulting file size, especially at low-speed. Relevant cycles, smaller than the complete one, can be used as alternative in the PG operation monitoring, provided that the signal contains the adequate information.

References

- [1] A. Purarjomandlangrudi, Acoustic Emission Condition Monitoring: An Application for Wind Turbine Fault Detection, *International Journal of Research in Engineering and Technology* (2)(2013) 907-918.
- [2] H. Chang, P. Borghesani, W.A. Smith, Z. Peng, Application of surface replication combined with image analysis to investigate wear evolution on gear teeth – A case study, *Wear* (430-431)(2019) 355-368.
- [3] R. Liu, H. Zuo, J. Sun, L. Wang, Electrostatic monitoring of wind turbine gearbox on oil-lubricated system, *Proceedings of the Institution of Mechanical Engineers, Part C: Journal of Mechanical Engineering Science* (231)(2019), pp. 3649-3664.
- [4] W. Cao, H. Zhang, N. Wang, H.W. Wang, Z.X. Peng, The gearbox wears state monitoring and evaluation based on on-line wear debris features, *Wear* (426–427)(2019), Part B pp. 1719-1728.
- [5] P. Kundu, A.K. Darpe, M.S. Kulkarni, A correlation coefficient based vibration indicator for detecting natural pitting progression in spur gears, *Mechanical Systems and Signal Processing* (129)(2019) 741-763.
- [6] M. Elforjani, D. Mba, A. Muhammad, A. Sire, Condition monitoring of worm gears, *Applied Acoustics*(73)(2012)(8) 859-863.
- [7] F. Elasha, C. Ruiz-Cárcel, D. Mba, G. Kiat, I. Nze, G. Yebra, Pitting detection in worm gearboxes with vibration analysis, *Engineering Failure Analysis* (42)(2014) 366-376.
- [8] M. Grzeszkowski, C. Gühmann, P. Scholzen, C. Löpenhaus, S. Nowoisky, G. Kappmeyer, Experimental study on the pitting detection capabilities for spur gears using acoustic emission and vibration analysis methods, *American Gear Manufacturers Association Fall Technical Meeting* (2018)
- [9] T. Toutountzakis, C. K. Tan, D. Mba, Application of acoustic emission to seeded gear fault detection, *NDT and E International* (38)(1)(2005) 27-36.
- [10] E. Caso, A. Fernandez-del-Rincon, P. Garcia, M. Iglesias, F. Viadero, Monitoring of misalignment in low speed geared shafts with acoustic emission sensors, *Applied Acoustics* (159)(2019).

- [11] Z. Geng, D. Puhan, T. Reddyhoff, Using acoustic emission to characterize friction and wear in dry sliding steel contacts, *Tribology International* (134)(2019) 394–407.
- [12] A.B. Novoa, C.M. Vicuna, New aspects concerning the generation of acoustic emissions in spur gears, the influence of operating conditions and gear defects in planetary gearboxes, *Insight - Non-Destructive Testing and Condition Monitoring* (58)(10)(2016) 18-27.
- [13] C.K. Tan, D. Mba, Identification of the acoustic emission source during a comparative study on diagnosis of a spur gearbox, *Tribology International* (38)(5)(2005) 469-480.
- [14] B. Eftekharnjad, D. Mba, Seeded fault detection on helical gears with acoustic emission, *Applied Acoustics* (70)(4)(2009) 547-555.
- [15] T. Toutountzakis, D. Mba, Observations of acoustic emission activity during gear defect diagnosis, *NDT and E International* (36)(7)(2003) 471-477.
- [16] C. K. Tan, P. Irving, D. Mba, A comparative experimental study on the diagnostic and prognostic capabilities of acoustics emission, vibration and spectrometric oil analysis for spur gears, *Mechanical Systems and Signal Processing* (21)(1)(2007) 208-233.
- [17] C. Scheer, W. Reimche, F. Bach, Early fault detection at gear units by acoustic emission and wavelet analysis, *J. Acoust. Emission* (25)(2007) 331-340.
- [18] L. Gao, F. Zai, S. Su, H. Wang, P.Chen, L. Liu, Study and application of acoustic emission testing in fault diagnosis of low-speed heavy-duty gears, *Sensors* (11)(1)(2011) 599-611.
- [19] T. H. Loutas, D. Roulias, E. Pauly, V. Kostopoulos, The combined use of vibration, acoustic emission and oil debris on-line monitoring towards a more effective condition monitoring of rotating machinery, *Mechanical Systems and Signal Processing* (25)(4)(2011) 1339-1352.
- [20] P.Feng, P. Borghesani, H. Chang, W.A. Smith, R. B Randall, Z Peng, Monitoring gear surface degradation using cyclostationarity of acoustic emission, *Mechanical Systems and Signal Processing* (131)(2019) 199–221.

- [21] J. Yoon, D. He, Planetary gearbox fault diagnostic method using acoustic emission sensors, *IET Science, Measurement and Technology* (9)(8)(2015) 936-944.
- [22] F. Elasha, M. Greaves, D. Mba, D. Fang, A comparative study of the effectiveness of vibration and acoustic emission in diagnosing a defective bearing in a planetary gearbox, *Applied Acoustics* (115)(2017) 181-195.
- [23] J. Sanchez-Espiga, A. Fernandez-del-Rincon, M. Iglesias, F. Viadero, Influence of errors in planetary transmissions load sharing under different mesh phasing, *Mechanism and Machine Theory* (153)(2020).
- [24] W. Bartelmus, R. Zimroz, Vibration spectra characteristic frequencies for condition monitoring of mining machinery compound and complex gearboxes, *Prace Naukowe Instytutu Gornictwa Politechniki Wroclawskiej* (40)(133)(2011) 17-34.
- [25] Fernández del Rincón, A., Cerdá, R. et Al, Test Bench for the Analysis of Dynamic Behavior of Planetary Gear Transmissions”, *Advances in Condition Monitoring of Machinery in Non-Stationary Operations*, 2014, Springer Berlin Heidelberg, pages=“485-495”, isbn=“978-3-642-39348-8
- [26] P. Theobald, B. Zeqiri, J. Avison, Couplants and their influence on AE sensor sensitivity, *Journal of Acoustic Emission* (26)(2008) 91-97.
- [27] E. Bechhoefer, Y. Qu, J. Zhu, D. He, Signal Processing Techniques to Improve an Acoustic Emissions Sensor, *PHM 2013 - Proceedings of the Annual Conference of the Prognostics and Health Management Society* (4)(2013) 581-588.
- [28] P. Borghesani, W.A. Smith, X. Zhang, P. Feng, J. Antoni, Z. Peng, A new statistical model for acoustic emission signals generated from sliding contact in machine elements, *Tribology International* (127)(2018) 412-419.
- [29] V.A. Belyi, O.V. Kholodilov, A.I. Sviridyonok, Acoustic spectrometry as used for the evaluation of tribological systems, *Wear* (3)(69)(1981) 309-319.

- [30] k. Sugiyama, T. Matsuo, Evaluation of the surface condition of spur gears using the acoustic emission method, *Materials Transactions* (12)(60)(2019) 2542–2551.
- [31] C. Ferrer, F. Salas, M. Pascual, J. Orozco, Discrete acoustic emission waves during stick-slip friction between steel samples, *Tribology International* (1-2)(43)(2010) 1-6.
- [32] J.M.M.A. Araújo, S. J. Wilcox, R. L. Reuben, Investigation of the role of dislocation motion in the generation of acoustic emission from metal cutting, *Proceedings of the Institution of Mechanical Engineers, Part B: Journal of Engineering Manufacture* (12)(223)(2009) 1507-1518.
- [33] A. Qu, B. VanHecke, D. He, J. Yoon, E. Bechhoefer, A Study on Comparing Acoustic Emission and Vibration sensors for Gearbox Fault Diagnostics, *Conference: Machinery Failure Prevention and Technology - Virginia Beach VA* (2014)
- [34] S. Hutt, A. Clarke, H.P. Evans, Generation of Acoustic Emission from the running-in and subsequent micropitting of a mixed-elastohydrodynamic contact, *Tribology International* (119)(2018) 270–280.
- [35] J. Miettinen, P. Andersson, Acoustic emission of rolling bearings lubricated with contaminated grease, *Tribology International* (33)(2000) 777–787.
- [36] A. B. Novoa, C.M. Vicuña, New Aspects Concerning the Generation of Acoustic Emissions (AE) in Spur Gears and the Influence of Operating Conditions, *Surveillance - 7 International Conference* (2013) 1-13.
- [37] C.M. Vicuña, C. Höweler, A method for reduction of Acoustic Emission (AE) data with application in machine failure detection and diagnosis, *Mechanical Systems and Signal Processing* (97)(2017) 44-58.